Gyrokinetic simulation of dissipative trapped electron mode in tokamak edge

C. Zhao, T. Zhang, and Y. Xiao[a)]
Institute for Fusion Theory and Simulation, Zhejiang University, Hangzhou 310027, China

(Received 2 February 2017; accepted 13 April 2017; published online 9 May 2017)

The gyrokinetic simulation using the gyrokinetic toroidal code (GTC) is carried out for the dissipative trapped electron mode (DTEM), which is an important source for the electrostatic turbulence in the pedestal of tokamak plasmas. The DTEM instability is identified for the edge plasmas, and its dependence on the wavelength and collisional frequency is obtained by both simulation and theory. It is shown for the first time that the linear gyrokinetic simulation results are fully consistent with that from the analytic theory with edge parameters. This suggests that the GTC code can simulate accurately the DTEM instability in the pedestal. It provides a useful benchmark for verifying gyrokinetic simulation of edge plasmas. *Published by AIP Publishing*. [http://dx.doi.org/10.1063/1.4982816]

I. INTRODUCTION

Low frequency drift-wave turbulence induced by plasma pressure gradient is an important candidate for anomalous transport in tokamaks. In particular, turbulence driven by trapped electron instabilities, namely, collisionless trapped electron mode (CTEM) and dissipative trapped electron mode (DTEM), can be responsible for the radial electron transport in tokamak plasmas. The CTEM, excited by precessional resonance of the magnetically trapped electrons, has been extensively investigated by analytical theory[1,2] and gyrokinetic simulation.[3–6] Much understanding related to physics of the DTEM have been gained, in particular, its linear instability properties, nonlinear saturation, and transport characteristics. On the other hand, the DTEM in the tokamak pedestal region is less understood.[7] Using a simple Krook collision operator, Cheng and Chen presented a linear theory of DTEM for the instability condition and two dimensional mode structures.[8] Recently, the interest on the DTEM has been revived by the observation of the so-called edge coherent mode (ECM) observed in the Experimental Advanced Superconducting Tokamak (EAST).[9] In the H-mode regime, the DTEM can play an important role in the pedestal region since (1) the population of the trapped electrons increases with radius and maximizes near the plasma edge, (2) the edge plasma temperature drops rapidly and becomes so low that the collisions cannot be ignored, and (3) the pressure profile is so steep that the resonant interaction between the drift waves and the trapped electrons is rather weak. In this work, we use the gyrokinetic code GTC[10] to investigate the linear physics of DTEM in the tokamak pedestal. For the first time, the pedestal DTEM simulations are fully consistent with the analytical theory that includes the pitch angle scattering collisions. This suggests that the GTC code can simulate accurately the DTEM instability for tokamak edge plasmas. Accordingly, the GTC code should be useful for simulating the DTEM turbulence at the tokamak edge, where the plasma has sharp gradients and collisions are important. In addition, this work provides an ideal example to benchmark the capability of the gyrokinetic code in simulating the DTEM instability in the tokamak edge.

This paper is organized as follows. In Sec. II, we discuss the simulation model and parameters. Then, the results for the DTEM obtained from the GTC simulation are presented and compared with an analytic theory in Sec. III. The analytical theory is given in detail in Sec. IV. Finally, the discussions and conclusions are given in Sec. V.

II. SIMULATION MODEL AND PARAMETERS

The GTC code is a three-dimensional global gyrokinetic particle code using the Boozer coordinates for general magnetic field geometry in tokamaks.[10] The GTC code invokes a nonlinear δf scheme[11] for investigating waves and instabilities, turbulence, neoclassical transport, and other important physics in tokamaks.[12,13] The GTC code has a low particle noise level due to the use of the δf scheme and a field-aligned mesh. The implementations of a gyrokinetic Poisson solver[14] suitable for general magnetic field geometry and guiding center equations of motion[15] in magnetic coordinates[16] enable the code to efficiently simulate physics phenomena in many magnetic confinement devices using realistic numerical plasma equilibria. In order to simulate the sharp gradient tokamak edge, we use a uniform particle loading method to avoid the sharp temperature and density variation in the simulation domain, while keeping the real gradient in weight pushing equation.[14] The code is truly global as it solves the gyrokinetic Poisson equation in real space and has the unique capability to simulate a full poloidal cross section using zero radial boundary conditions. The finite difference method based on an unstructured mesh is used in the current version of GTC,[14] and the FEM Poisson and Maxwell solver[17,18] is under development. It has been rigorously benchmarked against the existing analytic theories and other gyrokinetic simulations for important issues such as neoclassical transport[19] and turbulent transport.[14,20] In particular, the linear frequency and growth rate of the ion temperature gradient (ITG) mode and collisionless trapped electron mode (CTEM) have been shown to agree well with other codes for the tokamak core plasmas.[4]

[a)]Author to whom correspondence should be addressed. Electronic mail: yxiao@zju.edu.cn

In the GTC simulation, the particle distribution is decomposed into an equilibrium Maxwellian distribution F_0 and a perturbed distribution function δf. The latter one for ions, i.e., δf_i, is given by the gyrokinetic equation

$$\left[\frac{\partial}{\partial t}+\left(v_{||}\hat{b}+\mathbf{v}_d\right)\cdot\nabla\right]\delta f_i = -\left(\mathbf{v}_E\cdot\kappa_{pi}+\frac{Z_i e}{T_i}v_{||}E_{||}-\frac{Z_i e}{T_i}\mathbf{v}_d\cdot\nabla\delta\phi\right)F_{0i}, \quad (1)$$

where Z_i is the ion charge number, $\mathbf{v}_d=\mathbf{v}_g+\mathbf{v}_c=v_{||}^2\nabla\times\hat{b}/\omega_{ci}+\mu\hat{b}\times\nabla B_0/(m\omega_{ci})$ is the sum of the ∇B and curvature drift velocity, $\mathbf{v}_E=c\hat{b}\times\nabla\delta\phi/B_0$ is the $E\times B$ drift velocity and $\delta\phi$ is the perturbed electric potential, $\hat{b}\equiv\mathbf{B}_0/B_0$ is the unit vector along the field line, μ is the magnetic momentum of particles, and B_0 represents the equilibrium magnetic field, $\omega_{ci}=Z_i eB_0/m_i c$ is the ion gyro frequency, and $\kappa_{ps}\equiv\nabla\ln n_0+[m_s v^2/(2T_s)-3/2]\nabla\ln T_s$ with $s=i,e$ represents the ion or electron pressure gradient.

The perturbed electron distribution δf_e consists of an adiabatic response $\delta f_e^{(0)}=e\delta\phi F_0/T_e$ and non-adiabatic response δg_e that satisfies the drift kinetic equation

$$\left[\frac{\partial}{\partial t}+\left(v_{||}\hat{b}+\mathbf{v}_d\right)\cdot\nabla-C_{ei}\right]\delta g_e = -F_{0e}\left[\mathbf{v}_E\cdot\nabla\ln F_{0e}+\frac{\partial}{\partial t}\left(\frac{e\delta\phi}{T_e}\right)-\mathbf{v}_d\cdot\nabla\left(\frac{e\delta\phi}{T_e}\right)\right]. \quad (2)$$

The δf method used in the GTC efficiently limits the Monte Carlo noise associated with the numerical particles. We denote $w_i=\delta f_i/f_i, w_e=\delta f_e/f_e$, so that one can write

$$\frac{d}{dt}w_i=-\left(\mathbf{v}_E\cdot\kappa_{pi}+\frac{Z_i e}{T_i}v_{||}E_{||}-\frac{Z_i e}{T_i}\mathbf{v}_d\cdot\nabla\delta\phi\right), \quad (3)$$

$$\frac{d}{dt}w_e=-\left[\mathbf{v}_E\cdot\kappa_{pe}-\frac{e}{T_e}\mathbf{v}_d\cdot\nabla\delta\phi+\frac{\partial}{\partial t}\left(\frac{e\delta\phi}{T_e}\right)\right]. \quad (4)$$

The collisions on the electrons are dominated by the electron-ion collisions, which can be represented for simplicity by a pitch angle scattering operator, given by the following Monte-Carlo process[21,22]

$$\xi_{t+\Delta t}=\xi_t(1-\nu_{ei}\Delta t)+(R_n-0.5)\sqrt{12(1-\xi_n^2)\nu_{ei}\Delta t}, \quad (5)$$

where $\xi=v_{||}/v$ is the pitch angle of the particle motion, Δt is the time step, and R_n is a random number uniformly distributed between 0 and 1 at the nth time step.

For simplicity, we shall assume concircular flux surfaces. The tokamak edge parameters are $R_0/L_{Ti}=69.2$, $R_0/L_{Te}=69.2$, $R_0/L_n=69.2$, $m_i/m_e=1837$, $q=0.85+1.10r/a+1.00(r/a)^2, \varepsilon=0.3$, $n=26$, where $L_{Ts}=1/\partial_r\ln T_s$ with $s=i,e$ is the scale length of the temperature gradient, $L_n=1/\partial_r\ln n$ is the scale length of the density gradient, $\varepsilon=a/R_0$ with R_0 the major radius of the tokamak, a is the minor radius of the tokamak, and r is the radial coordinate. The toroidal magnetic field is defined by $B_T=B_0/[1+(r/a)\cos(\theta)]$, with θ the poloidal angle. The mesh for the electromagnetic field perturbations consists of 32 or 64 grids in the parallel or toroidal direction, and hundreds of grids in the poloidal direction on each flux surface. An unstructured poloidal mesh is used with grid size about $0.5\rho_i$ or $1.0\rho_i$ in the radial or poloidal directions to simulate the short perpendicular-wavelength modes.

III. GYROKINETIC SIMULATION RESULTS FOR EDGE DTEM

Figs. 1(a) and 1(b) show the electrostatic potential on the poloidal plane for plasma without collisions and with collisions, respectively. For the collisional case, the effective collisional frequency is $\nu_e^*=0.2$, with $\nu_e^*=\nu_{Te}qR_0/v_{the}\varepsilon^{3/2}$ where the typical electron collisional frequency $\nu_{Te}=\ln\Lambda n_i Z_i^2 e^4/4\pi\varepsilon_0^2 m_e^2 v_{the}^3$, $v_{the}\equiv\sqrt{2T_e/m_e}$ is the electron thermal velocity, $\ln\Lambda$ is the Coulomb logarithm, and ε_0 is the dielectric constant of the vacuum. As can be seen in Fig. 1(a), there is no unstable mode in the collisionless case. However, Fig. 1(b) shows that in the collisional case, an unstable DTEM mode is excited. The latter can be attributed to the dissipative response of the magnetically trapped electrons.[23] It is also found that the most unstable region is not the poloidal position with the worst curvature (around $\theta=0$). This unusual mode structure can be attributed to the strong pressure gradient in the pedestal region, where the magnetic drift frequency is much smaller than the diamagnetic frequency.[24]

Fig. 2 shows the dependence of the linear growth rate and real frequency on the poloidal wavelength. The solid curve is from the analytical theory given in Sec. IV, and the open circles are from our GTC simulation. One can see that the GTC results are fully consistent with that from the theory and the short-wavelength modes have higher growth rates than the long-wavelength modes, which shows that the GTC simulation model works properly for the tokamak pedestal. As shown in Fig. 2(a), the linear growth rate increases with $k_\theta\rho_s$, which is due to the finite Larmor radius effect in the non-adiabatic ion response.[23,25]

In Fig. 3, we scan the linear growth rate with various collisional frequencies. The collisional frequency is changed by solely varying the background electron density. One can see that the linear growth rate increases with the effective collision frequency for $\nu_e^*<1$, which is a typical signature of the DTEM instability. For the given parameters, the real

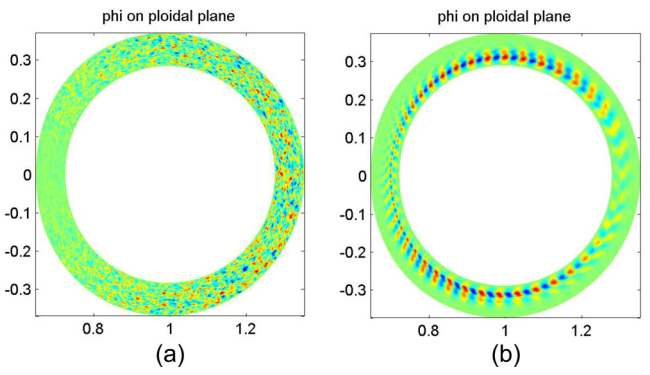

FIG. 1. Electrostatic potential on the poloidal plane for $\nu_e^*=0$ (a), $\nu_e^*=0.2$ with passing particle (b).

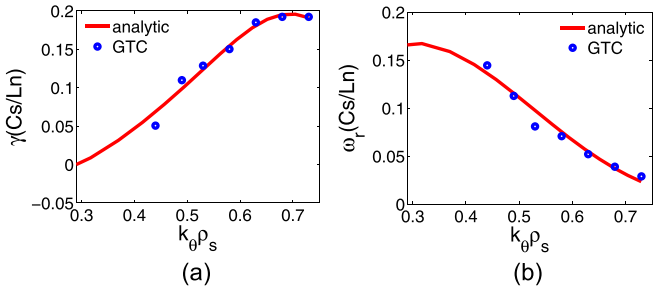

FIG. 2. Linear growth rate (a) and real frequency (b) vs. $k_\theta\rho_s$ for $\nu_e^* = 0.2$.

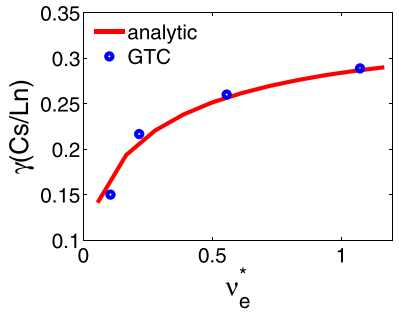

FIG. 3. Linear growth rate vs. ν_e^* for $k_\theta\rho_s = 0.6$.

frequency of the DTEM is wandering around $\omega_r \sim 0.1C_s/L_n$, which is roughly independent of the collision frequency and consistent with the theory given in Section IV.

Fig. 4 shows that at high collision frequency ($\nu_e^* > 1$), collisions can mitigate the growth of the short wavelength modes and enhance the growth of long wavelength modes. The electron response contains both dissipative and resonant components. It is found that the collisions destabilize the long wavelength mode, while damp the short wavelength mode. The physics mechanism requires further investigation. However, the theoretical model in Section IV is not suitable for $\nu_e^* > 1$, since the collision frequency becomes larger than the bounce frequency. Therefore, in Fig. 4, we show only the simulation results.

In Fig. 5, we show the linear DTEM growth rate vs. $\eta_e \equiv d\ln T_e/d\ln n_e = L_{ne}/L_{Te}$ and find that the growth rate increases linearly with the latter. This trend is similar to that of the CTEM,[4] while the underlying physics is different. In the DTEM, the instability is driven by the dissipative response of the bulk electrons,[26] which contains a component proportional to the temperature gradient or η_e. But in

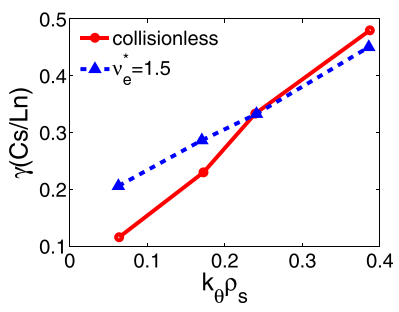

FIG. 4. Linear growth rate vs. $k_\theta\rho_s$ for $\nu_e^* = 1.5$ and collisionless ($\nu_e^* = 0.0$) with $R_0/L_{Ti} = 120$, $R_0/L_{Te} = 120$, and $R_0/L_n = 120$.

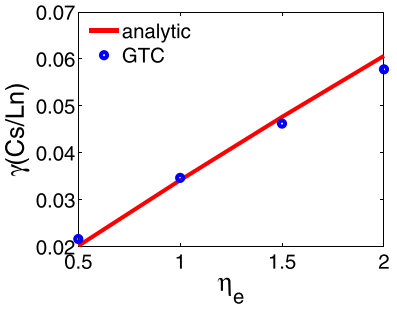

FIG. 5. Linear growth rate vs. η_e with $\nu_e^* = 0.1$, $k_\theta\rho_s = 0.1$, and other default parameters.

the CTEM, the instability is driven by toroidal precessional resonance, where the non-adiabatic response also contains a component proportional to the temperature gradient or η_e.

IV. DTEM THEORY FOR TOKAMAK EDGE

The theoretical results presented in Figs. 2 and 3 are from a gyrokinetic theory applied to the pedestal region,[27] where one assumes that $\omega \sim \omega_{*e} \gg \omega_{de}$, $\nu_e^i \ll \omega_{be}$. Here, ω_{*e} is the electron diamagnetic frequency, $\omega_{de} = \mathbf{k}_\perp \cdot \mathbf{v}_{de}$, and $\omega_{be} = \sqrt{\varepsilon}v_{the}/qR$ with the inverse aspect ratio $\varepsilon = r/R_0$. For convenience, the particle distribution function is expressed as

$$f_s = F_{0s} - \frac{e_s\delta\phi}{T_s}F_{0s} + \delta H_s e^{ik_\perp\rho_{Ls}}, \tag{6}$$

where F_{0s} is the equilibrium distribution function with $s = i, e$ for ions and electrons, respectively, $-e_s\delta\phi F_{0s}/T_s$ is the adiabatic part of the perturbed distribution function, δH_s is the non-adiabatic or kinetic part of the perturbed distribution function, $k_\perp$ is the wave vector perpendicular to the static magnetic field, $\rho_{Ls} = v_\perp/\omega_{cs}$ is the Larmor radius, and $\omega_{cs} = e_sB/m_sC$ is the gyro-frequency. In the long wavelength limit $k_\perp\lambda_e \ll 1$, the Poisson equation solved for the electrostatic field becomes the quasi-neutrality condition

$$\frac{n_0e^2\delta\phi}{T_e}\left(1 + Z_i^2\tau\right) = \langle Z_ieJ_0\delta H_i\rangle - \langle e\delta H_e\rangle, \tag{7}$$

where $J_0 = J_0(k_\perp\rho_i)$ is the zeroth order Bessel function, $\tau = T_e/T_i$, and $\langle\cdots\rangle$ denotes the integration over the velocity space. The collisions, parallel resonance, and magnetic drifts for the ions can be neglected in the low frequency limit $\omega \ll k_{||}v_{ti}$. Thus, δH_i has the following solution after simplifying the ion gyrokinetic equation

$$\delta H_i = -\frac{Z_ie}{T_e}\tau\left[1 + \frac{\omega_{*e}}{\omega}\left(1 + \eta_i\left(\frac{m_iv^2}{2T_i} - \frac{3}{2}\right)\right)\right]F_{0i}J_0(k_\perp\rho_i)\delta\phi, \tag{8}$$

where the electron diamagnetic frequency $\omega_{*e} = k_\theta T_eL_nc/eB$.

In tokamaks, the electrons can be separated into passing and trapped electrons. Accordingly, it is convenient to define a pitch angle variable $\kappa \equiv [E(1+\varepsilon) - \mu B_0]/2\varepsilon E$, where E is the kinetic energy of particles, for a large aspect ratio circular tokamak, such that $0 \le \kappa \le 1$ and $\kappa \ge 1$ correspond to the

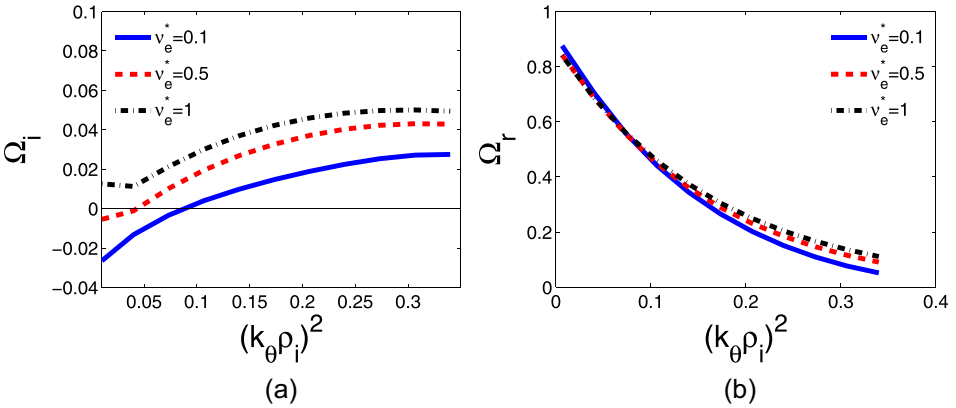

FIG. 6. Theoretical linear growth rate and real frequency vs. $(k_\theta\rho_i)^2$ for different collisional frequencies.

trapped and passing electrons, respectively. For the low frequency drift waves, the response of the passing electrons remains adiabatic. However, the kinetic response of the trapped electrons must be calculated from the kinetic equation, and it can be obtained conveniently by averaging the electron drift kinetic equation over their bounce orbit. Moreover, in the steep pressure gradient region, the magnetic drift can be ignored. For the electron-ion collisions, we use a pitch angle scattering or the Lorentz collision operator, which can also be bounce averaged. The electron distribution can then be obtained by solving the bounce averaged gyrokinetic equation[27]

$$\delta H_{etr} = -\frac{e\delta\phi}{T_e}Q(v)F_{oe}\left[1-\frac{J_0\left(2(1+i)\sqrt{\kappa/\nu_{eff}}\right)}{J_0\left(2(1+i)\sqrt{1/\nu_{eff}}\right)}\right], \quad (9)$$

$$\delta H_{ep} = 0, \quad (10)$$

where δH_{etr} is the kinetic distribution function for the trapped electrons, δH_{ep} is the kinetic distribution function for the passing electrons, v is the particle velocity, $Q(v) = 1 + \omega_{*e}/\omega \times [1 + \eta_e(m_e v^2/(2T_e) - 1.5)]$, ε is the inverse aspect ratio, $\nu_{eff} = \nu_e/\omega\varepsilon$, and $\nu_e = \ln\Lambda n_e e^4/4\pi\varepsilon_0^2 m_e^2 v^3$.

Inserting the ion and electron responses in Eqs. (8)–(10) in the quasi-neutrality condition, i.e., Eq. (7), and treating the ion as proton, i.e., $Z_i = 1$, one obtains the following integral equation for the pedestal DTEM dispersion relation:

$$\Omega - \frac{2\sqrt{2\varepsilon}}{\pi^{3/2}}\int_0^1 d\kappa K(\kappa)\int_0^\infty t^{\frac{1}{2}}e^{-t}\times\left(\frac{J_0\left(\sqrt{\kappa}x\right)}{J_0(x)}\right) \times\left\{\Omega-\left[1+\eta_e\left(t-\frac{3}{2}\right)\right]\right\}dt + \Omega\tau - (\Omega\tau+1)\Gamma_0(b) + \eta_i b(\Gamma_0(b)-\Gamma_1(b)) = 0, \quad (11)$$

where $t = m_e v^2/2T_e$, $x = 2(1+i)/\sqrt{\nu_{eff}}$, $\Omega = \omega/\omega_{*e}$, $b = (k_\perp\rho_i)^2 \equiv k_\perp^2 T_i/m_i\omega_{ci}^2$, $\Gamma_n = I_n(b)e^{-b}$, $n = 0,1$, and I_n is the nth order modified Bessel function. Instead of using the approximation given in Ref. 21, we can be more precise by numerically evaluating the integral on the left hand side of Eq. (11). Choosing the latter, Eq. (11) then becomes an algebraic equation from which the eigenvalue $\Omega \equiv \Omega_r + i\Omega_i$ can be obtained. The results are shown in Fig. 6 for $\varepsilon = 0.2$, $\nu_e^* = 0.1$, 0.5, 1, $\tau = 1$, $\eta_i = \eta_e = 1$, and $R_0/L_n = 69.2$. We see that for $\nu_e^* = 0.1$, the longer wavelength modes are stable, and as ν_e^* increases, the stable region becomes smaller. Fig. 6 also shows that the growth rate increases with $k_\theta\rho_i$, while the real frequency decreases with $k_\theta\rho_i$. The unstable mode propagates in the electron diamagnetic direction since $\Omega_r > 0$. One can see that Ω_r does not change much when ν_e^* increases from 0.1 to 1.0, confirming that the real frequency is mainly determined by the collisionless response of the electrons.

V. CONCLUSION AND DISCUSSION

In this section, we summarize our simulation and physics results as follows. We have used the GTC code to simulate the DTEM instability in the tokamak edge region. The gyrokinetic DTEM results are for the first time verified by an analytical theory for the edge region, which not only demonstrates that the GTC code can accurately simulate the DTEM instability but also provides a useful benchmark for the DTEM simulation in the edge region, where the plasma density and temperature gradients are steep and collisions can be the dominant destabilizing factor. The analytical model numerically integrates the trapped electron response and gives a more accurate DTEM dispersion relation. Our results show that for $\nu_e^* < 1$, the electron-ion collisions can drive the DTEM instability, and the shorter-wavelength modes are easier to excite than the long-wavelength modes. For weak collisions, even the long-wavelength modes can be stable. This may infer that the DTEM turbulence in the edge will have a relatively lower transport. The linear growth rate of DTEM increases linearly with η_e, a phenomenon similar to CTEM but with different physics mechanism. These linear verification studies provide a solid foundation for the gyrokinetic simulation to investigate the interesting nonlinear physics in the tokamak pedestal. In the future, we will use the GTC simulation to study the nonlinear saturation physics and transport physics of DTEM. Combining these future works with the results shown in this paper, we could achieve better understandings of the ECM (edge coherent mode) found in experiments.[9] Due to the steep gradient in the edge, the profile flattening effect could be significant in the nonlinear stage. Another difficulty may come from the pitch angle scattering operator, which does not conserve the particle momentum as is known.

ACKNOWLEDGMENTS

The work was supported by the National Magnetic Confinement Fusion Energy Research Program under Grant Nos. 2015GB110000 and 2013GB111000, China NSFC under Grant No. 11575158, and the Recruitment Program of Global Youth Experts. We thank Professor L. Chen and M. Y. Yu for useful discussions.

[1]J. Adam, W. Tang, and P. Rutherford, Phys. Fluids **19**, 561 (1976).
[2]P. J. Catto and K. T. Tsang, Phys. Fluids **21**, 1381 (1978).
[3]J. Lang, S. Parker, and Y. Chen, Phys. Plasmas **15**, 055907 (2008).
[4]G. Rewoldt, Z. Lin, and Y. Idomura, Comput. Phys. Commun. **177**, 775 (2007).
[5]Y. Xiao and Z. Lin, Phys. Plasmas **18**, 110703 (2011).
[6]L. Qi, J. Kwon, T. S. Hahm, and G. Jo, Phys. Plasmas **23**, 062513 (2016).
[7]D. R. Ernst, P. T. Bonoli, P. J. Catto, W. Dorland, C. L. Fiore, R. S. Granetz, M. Greenwald, A. E. Hubbard, M. Porkolab, M. H. Redi, J. E. Rice, K. Zhurovich *et al*., Phys. Plasmas **11**, 2637 (2004).
[8]C. Z. Cheng and L. Chen, Nucl. Fusion **21**, 403 (1981).
[9]H. Q. Wang, G. S. Xu, B. N. Wan, S. Y. Ding, H. Y. Guo, L. M. Shao, S. C. Liu, X. Q. Xu, E. Wang, N. Yan *et al*., Phys. Rev. Lett. **112**, 185004 (2014).
[10]Z. Lin, T. S. Hahm, W. W. Lee, W. M. Tang, and R. B. White, Phys. Plasmas **7**, 1857 (2000).
[11]A. M. Dimits and W. W. Lee, J. Comput. Phys. **107**, 309 (1993).
[12]Z. Lin, W. M. Tang, and W. W. Lee, Phys. Plasmas **2**, 2975 (1995).
[13]Y. Xiao and Z. Lin, Phys. Rev. Lett. **103**, 085004 (2009).
[14]Y. Xiao, I. Holod, Z. X. Wang, Z. Lin, and T. G. Zhang, Phys. Plasmas **22**, 022516 (2015).
[15]R. B. White and M. S. Chance, Phys. Fluids **27**, 2455 (1984).
[16]A. H. Boozer, Phys. Fluids **24**, 1999 (1981).
[17]P. Li, G. Zheng, and W. Zheng, Math. Methods Appl. Sci. **40**, 573 (2017).
[18]H. Duan, S. Li, R. Tan, and W. Zheng, J. Sci. Comput. **67**, 669 (2016).
[19]Z. Lin, W. M. Tang, and W. W. Lee, Phys. Rev. Lett. **78**, 456 (1997).
[20]W. Deng, Z. Lin, I. Holod, Z. Wang, Y. Xiao, and H. Zhang, Nucl. Fusion **52**, 043006 (2012).
[21]Z. Lin and W. W. Lee, Phys. Rev. E **52**, 5646 (1995).
[22]X. Q. Xu and M. N. Rosenbluth, Phys. Fluids **3**, 627 (1991).
[23]C. S. Liu, M. N. Rosenbluth, and W. M. Tang, Phys. Fluids **19**, 1040 (1976).
[24]H. S. Xie and Y. Xiao, Phys. Plasmas **22**, 090703 (2015).
[25]H. P. Qu, X. D. Peng, F. Wang, A. K. Wang, and Y. Shen, Phys. Plasmas **23**, 092511 (2016).
[26]B. B. Kadomtsev and O. P. Pogutse, Dokl. Akad. Nauk SSSR **186**, 553 (1969).
[27]J. W. Connor, R. J. Hastie, and P. Helander, Plasma Phys. Controlled Fusion **48**, 885 (2006).